Fracture Mechanics of Concrete Structures, de Borst et al (eds) © 2001 Swets & Zeitlinger, Lisse, ISBN 90 2651 825 0

Computational Fracture Analysis of Concrete Gravity Dams Toward Engineering Evaluation of Seismic Safety

Hideyuki Horii & Shue-Cheng Chen
Department of Civil Engineering, The University of Tokyo, Japan

From a point of view to utilize fracture mechanics of concrete for the solution of engineering problems, problems in crack modeling, computational algorithm, and damping implementation are discussed in conjunction with safety assessment of concrete dam against large earthquake. It is shown that the formulation for the crack-embedded element has an analogy with that of computational plasticity. This analogy enables us to utilize the return-mapping algorithm well established in computational plasticity for the dynamic analysis of crack growth in concrete. The ways of implementing damping to avoid diffused cracking are presented and simple examples of numerical analysis are shown to demonstrate the effect of damping and the performance of appropriate damping implementation for cracked elements.

1 INTRODUCTION

A long time has passed since fracture mechanics is applied to concrete and concrete structures and a great number of studies on modeling and numerical methods for crack growth in concrete have been carried out. It is at a stage to utilize the accumulated knowledge to solve real engineering problems. In this paper, a problem of safety assessment of a concrete dam against large earthquakes is selected as an example and issues on computational method necessary to the safety assessment are discussed.

1.1 *Crack growth in concrete dam under large earthquake excitation*

After Kobe earthquake in 1995, safety assessment and design of structures against large earthquake had become national concern in Japan. Dam is one of important structures on which a number of human lives are relied. Since the safety margin reserved in the existing dams is large, they are considered to be safe even against an earthquake larger than that expected in their design. However, it is important to clarify the reserved safety and to establish a new design method against larger earthquakes.

First thing to be done is the identification of critical states that lead to the collapse of dam or loss of reservoir under large earthquake excitation. In the case of concrete dam, one of them is the dynamic growth of cracks and its penetration of the dam body. The existing design method of concrete dam is based on the concept that no crack is allowed under earthquake excitation. However, it is possible that cracks are formed and propagated up to a certain point in the dam body during earthquake. The role of computational fracture mechanics of concrete is to predict the dynamic crack growth in concrete dam under large earthquake excitation.

1.2 *Method of safety assessment and anti-earthquake design*

Before problems of dynamic crack growth analysis are discussed, it is better to overview how the results of dynamic crack growth analysis are to be used for safety assessment and anti-earthquake design of concrete dam. Although the presented method is a proposal and is not officially adopted, the role and importance of computational method shall be understood.

For a concrete gravity dam, for example, under consideration, one may determine input earthquake excitation, time history of ground acceleration. Keeping the same waveform, the magnitude of excitation is varied with a parameter, for example, maximum ground acceleration. With given dynamic tension softening curve of dam concrete, elastic properties and damping ratio of concrete and rock foundation, the dynamic analyses of crack growth in concrete dam are carried out. For a given value of maximum ground acceleration, the minimum value of ligament ratio, which is the ratio of ligament length to the whole crack path, during the earthquake excitation

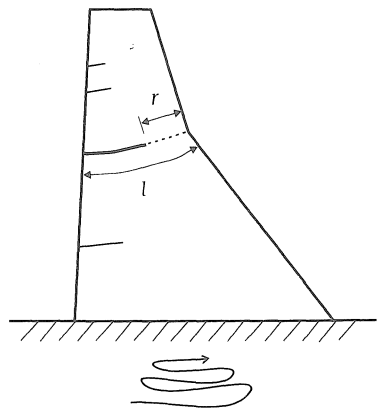

Figure 1: Main crack which forms and propagates in dynamic analysis of concrete gravity dam against large earthquake excitation

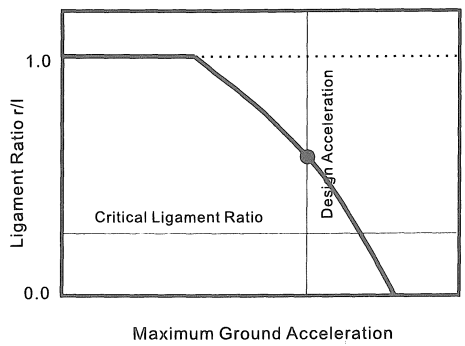

Figure 2: Ligament ratio as a function of input maximum ground acceleration

is obtained; see Fig. 1. The crack path is determined with a larger maximum ground acceleration when the crack passes through the dam body.

The obtained ligament ratio is plotted against the maximum ground acceleration as shown in Fig. 2. The role of the employed computational method is to prepare this figure. The accuracy of the computational method affects the curve in Fig. 2. Based on this result, the safety of the concrete gravity dam under consideration is evaluated in the following way.

The design maximum ground acceleration is determined, for example, as the maximum value expected for a period of 10,000 years. The value is plotted as a vertical line in Fig. 2. The Fig. 2 itself represents the extent of safety ensured for the considered dam. To quantify the ensured safety, one may define an index like the ligament ratio with the maximum earthquake excitation in 10,000 years and make a judgment comparing the value with the critical ligament ratio. If one is designing a new dam against large earthquake, Fig. 2 is used to determine the design variables so that, for example, the ligament ratio with the maximum earthquake excitation in 10,000 years is larger than the critical ligament ratio.

It is clear that the safety assessment requires a number of engineering judgments and knowledge related to the selection of input excitation, the design value of maximum ground acceleration, the critical ligament ratio, and so on. Those are very important issues, but they are out of scope of this paper.

1.3 *Problems in dynamic analysis of crack growth in concrete dam*

Damping is very important in dynamic analysis of a concrete dam to reproduce realistic behaviors of the dam. The damping to be used in the analysis consists of internal damping and radiation damping. The latter one is due to interaction among the dam body, the rock foundation, and the stored water. The value of damping to be used is not small and the damping creates a serious problem in the analysis of crack growth leading to the diffused cracking as discussed later.

The appropriate value of damping depends on how the dynamic analysis of concrete dam is carried out since the radiation damping is virtual one introduced to represent the effect of three dimensional interaction among the dam body, the rock foundation, and the stored water.

Ariga et al. (2000) carried out two-dimensional and three-dimensional dynamic analysis of a concrete gravity dam to reproduce data measured during actual earthquake motions. They determined dynamic properties for four different models. Here results for two models are briefly introduced.

Model 1 shown in Fig. 3 (a) is a two-dimensional dam body on a rigid foundation. Model 2 shown in Fig. 3 (b) consists of three dimensional dam body, rock foundation and stored water with viscous boundary along the side boundaries. The determined parameters are presented in Table 1.

It is seen from Table 1 that the damping constant used to obtain the maximum acceleration at the top of the dam close to the measured value is 20% that is very large. Even in model 2 without radiation damping, the damping constant is 5% that is not small.

Table 1: The damping ratios used to obtain the maximum acceleration at the top of the dam close to the measured value in Ariga et al. (2000)

Case	Max Accel	Damping ratio for dam			Damping ratio for rock		
	(m/sec^2)	Total	Material	Radiation	Total	Material	Radiation
Measurement	77.3	–	–	–	–	–	–
Model 1	74.3	20%	5%	15%	–	–	–
Model 2	80.0	5%	5%	0%	5%	5%	0%

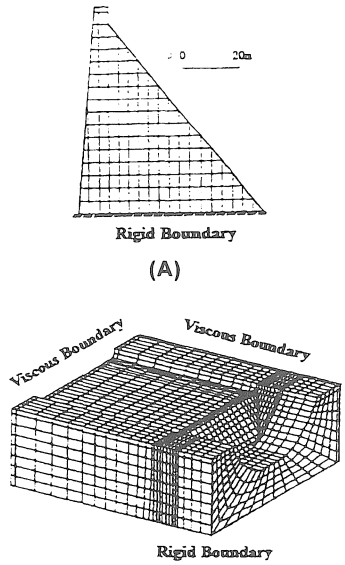

Figure 3: The FEM Models in Ariga et al. (2000): (a) 2D dam body on rigid foundation, (b) integral of 3D dam body, rock foundation, and stored water with viscous boundary along the side boundaries

Since the damping is indispensable in the dynamic analysis of concrete dam, the diffused cracking due to the artificial tension resistance by the damping is essential in the dynamic analysis of crack growth in concrete dams. An example of the diffused cracking is shown in Fig. 4. The damping implementations employed in the existing studies on dynamic analysis of crack growth in concrete dam are reviewed in 2.2.

Problems in crack modeling and algorithm for the analysis of crack growth in concrete are not specific to the dam problem. However, those issues are important to obtain accurate results such as those shown in Fig. 2 and to evaluate the safety of a concrete dam based on them. Problems related to crack modeling are discussed in 2.1. In the present paper, a crack-embedded element is employed and its formulation is presented in Section 3. It is emphasized that the crack-embedded element has a beneficial feature that the formulation has an analogy with that of computational plasticity. This analogy enables us to utilize algorithms developed for computational plasticity.

Those who have carried out crack growth analysis in concrete may all recognize the importance of a robust algorithm. In the numerical analysis of crack growth in concrete, loading (increasing crack opening with decreasing stress) or unloading (decreasing or frozen crack opening with decreasing stress) must be judged and different tangential stiffness, for example, must be assigned for all points of cracks. It is possible that a crack assumed to be loading undergoes unloading and vice versa in the scheme of computational loops and convergence with consistent combination of loading and unloading cracks cannot be obtained.

All numerical works of crack growth in concrete seem to employ certain measures to overcome this difficulty, but not many papers discuss the employed algorithm. In the present paper, an analogy between the formulation of computational plasticity and that of the crack-embedded element is presented, and the return-mapping algorithm well established in computational plasticity is employed for the dynamic analysis of crack growth in concrete in Section 3.

2 CRACK MODELING AND DAMPING IMPLEMENTATION

Toward evaluation of seismic safety of concrete gravity dams, the role of computational fracture analysis is to provide the information about the dynamic crack growth in dams under large earthquake excitation, which is presented as the ligament ratio-earthquake intensity (maximum ground acceleration, for example) curve shown in Fig. 2.

In this section, we shall briefly review two important problems which strongly affect the information about the dynamic crack growth in dams provided by computational seismic fracture analyses—the problems of crack modeling and damping implementation.

2.1 *Problems of Crack Modeling*

A crack in concrete is a very narrow region in which the mechanical properties of uncracked concrete lose their original strength due to significant damage or complete separation. These unique characteristics impose special difficulties on the conventional C_0 finite element method. Different approaches have been developed to model cracks in the context of finite element method and applied to fracture analysis of concrete gravity dams.

2.1.1 *Smeared crack models and stress locking*

Smeared crack model is a *continuum crack model* which models the effect of cracks by constitutive relationship of the cracked continuum without explicit kinematic representation of cracks. The behavior of cracked concrete can be described in terms of stress-strain relations and, upon cracking, it is sufficient to replace the initial isotropic stress-strain relation by an orthotropic stress-strain relation. Smeared crack model has been popularly used in seismic fracture analysis of gravity dams for a long time (Tinawi et al. 2000; Ghaemian and Ghobarah 1999; Léger and Leclerc 1996; Bhattacharjee and Léger 1993; El-Aidi and Hall 1989).

The problem for smeared crack models is *stress locking*—spurious stress transfer across a widely open

crack. The spurious stress transfer is caused by a poor kinematic representation of the discontinuous displacement field around a crack. Unless the direction of the crack (represented by a band of cracking elements) happens to be parallel to element sides, smeared crack models generate cohesive forces acting across the crack even at very late stages of the cracking process when the crack should be completely stress-free (Jirásek 2000).

2.1.2 *Isotropic damage models and isotropy*

Isotropic damage model (and isotropic damage-plastic model) is also a continuum crack model without explicit kinematic representation of cracks. A scalar damage variable D ($0 \leq D \leq 1$) is used to "degrade" the stiffness of concrete under cracking; when the crack completely separates, D becomes 1 which represents the cracked concrete lose all its capacity to transfer tension stresses. This approach has been favored in recent research papers on seismic fracture analysis of gravity dams, because its formulation can include complicated material behaviors of concrete (fracture due to tension and compression, stiffness degradation and recovery due to cyclic load, rate-dependent effects) in a thermodynamically consistent way (Lee and Fenves 1998; Faria et al. 1998; Cervera et al. 1996; Cervera et al. 1995).

Isotropic damage model does not exhibit the stress locking problem in smeared crack methods because it has no specific orientation for cracking effects—the stiffness in all direction becomes zero when the crack completely separates. On the other hand, since a crack in concrete is restricted in a very narrow region, if we check the *gross* mechanical properties of the material around the crack (or the area of the finite elements surrounding a crack), it does exhibit strong anisotropy. The tension stiffness in the normal direction is significantly weakened by the crack, but the stiffness in the tangent direction virtually does not change. The isotropic damage model cannot exhibit anisotropy.

2.1.3 *Discrete crack models and the necessity of remeshing*

Conventional discrete crack model (Hillerborg et al. 1976) explicitly models crack as a displacement discontinuity with certain cohesive traction-separation rule. The kinematic path of crack is explicitly specified and becomes part of the boundary of the finite element mesh. If the crack path is known beforehand, the concept of the discrete crack model is relatively simple and effective—it does not suffer from the problem of stress locking and it exhibits anisotropy naturally.

Normally, the crack path is one of the major unknowns in fracture analysis. Following up the evoluting crack path, we need to keep updating the mesh (*remeshing*) to accommodate the newly appearing boundaries. Despite its simplicity and effectiveness in modeling cracking behavior, the discrete crack model has been seldom adopted in recent research papers on seismic analysis of concrete gravity dams because of the necessity of remeshing procedure.

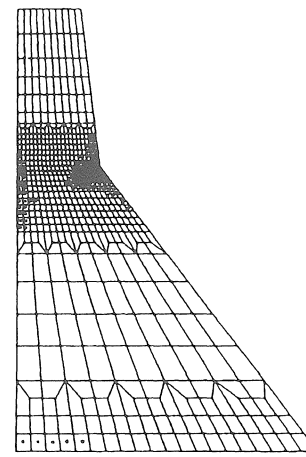

Figure 4: Crack diffusion caused by the conventional implementation of stiffness-proportional damping, adapted from Bhattacharjee and Léger (1993)

2.2 *Problems of Damping Implementation*

In the literature of seismic fracture analysis of gravity dams, a *stiffness-proportional damping* is normally adopted; the *mass-proportional damping* in Rayleigh's damping is neglected by the reason that it has no physical basis (Lee and Fenves 1998, p. 947) or it would provide some artificial stability to the portion of the dam above a crack (El-Aidi and Hall 1989, p. 840).

The conventional implementation of stiffness-proportional damping is only dominated by the deformation rate of each element (defined by the relative velocities of nodes) because a constant stiffness matrix is used. When an element is cracking, the deformation rate of this element could significantly increase so that large artificial tension resistance is generated across the cracked element. This artificial resistance results in unreal *diffused cracks* in the cases where cracking should be highly localized, see the example in Fig. 4. Three ways have been exploited to solve this problem: (1) setting the damping of cracked elements to zero (El-Aidi and Hall 1989), (2) defining the damping by tangent stiffness matrix instead of the elastic stiffness matrix (Bhattacharjee and Léger 1993), (3) in isotropic damage model, defining the damping locally to be proportional to the degraded stiffness (Lee and Fenves 1998).

On the other hand, the usage of Rayleigh's damping is to adjust the weight between the mass-proportional damping and stiffness-proportional damping in order to preserve a specified range of vibration modes and damps out the others (Clough and Penzien 1993, p. 235). Considering the overall dynamic response of the system, it could be questionable to neglect mass-proportional damping. If the mass-proportional damping is to be included, its effect on the cracked elements needs further examination.

3 CRACK-EMBEDDED ELEMENT AND ANALOGY WITH COMPUTATIONAL PLASTICITY

As we have mentioned in the previous section, despite its simplicity and effectiveness in modeling cracking behavior, the discrete crack model is seldom adopted in recent research papers on seismic analysis of concrete dams because remeshing procedure is necessary when crack path is not known beforehand. This difficulty can be removed and simultaneously the simplicity and effectiveness of the discrete crack model can be preserved by the recently emerging *crack-embedded elements* (Oliver 1996; Armero and Garikipati 1996).

Crack-embedded elements model crack by a displacement discontinuity embedded *inside* a standard displacement-based finite element. Since crack paths need not evolve along the element sides, no remeshing procedure is required. Moreover, for its discrete-crack nature, a crack-embedded element naturally exhibits the anisotropy caused by crack (contrary to scalar damage models) and does not suffer from stress locking (contrary to smeared-crack models).

From an algorithmic point of view, we have noted that the formulation of the crack-embedded elements (Oliver 1996; Armero and Garikipati 1996) is analogous to the one-dimensional classical theory of plasticity (Simo and Hughes 1998, Chapter 1). This fact suggests that we could *emulate the return-mapping algorithms (and their restrictions) well-established in computational plasticity* to develop robust and efficient algorithms for crack-embedded elements.

In this section, the analogy of the formulation of crack-embedded elements to that of one-dimensional plasticity is demonstrated by a one-dimensional crack-embedded element, then a return-mapping algorithm and implementation of damping for this element is developed, at last the extension to two-dimensional crack-embedded elements is briefly described. The detailed development of the algorithm and proofs are presented in Chen and Horii (2001).

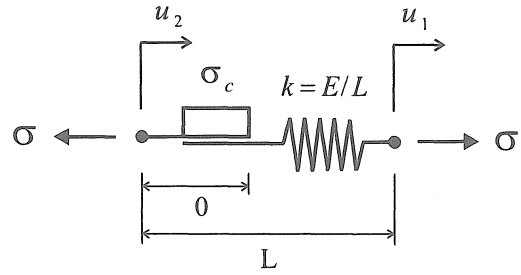

Figure 5: One-Dimensional Crack-Embedded Element

3.1 *One-Dimensional Crack-Embedded Element*

Consider a one-dimensional finite element shown in Fig. 5, which initially possesses length L (and unit area) and consists of a spring of Young's modulus E (elastic constant $k = E/L$) and a Coulomb friction element of initial sliding stress $\sigma_c > 0$; the Coulomb friction element, representing a crack, does not occupy length until it starts to slide (open).

First, observe that stress σ can be expressed by the difference of two strain terms

$$\begin{aligned}\sigma &= k\,[(u_1 - u_2) - \alpha] \\ &= E\left[\left(\frac{u_1}{L} - \frac{u_2}{L}\right) - \frac{\alpha}{L}\right] \\ &= E\,[\varepsilon - \tilde{\varepsilon}] \qquad (1a) \\ &= E\,[\mathbf{B}\mathbf{u} - G\alpha] \qquad (1b)\end{aligned}$$

in which the strain terms ε and $\tilde{\varepsilon}$ are defined as

$$\varepsilon \equiv \frac{u_1}{L} - \frac{u_2}{L} = \left\langle \frac{1}{L} \; -\frac{1}{L} \right\rangle \begin{Bmatrix} u_1 \\ u_2 \end{Bmatrix} = \mathbf{B}\mathbf{u}, \qquad (2a)$$

$$\tilde{\varepsilon} \equiv G\,\alpha, \quad G = 1/L. \qquad (2b)$$

Note that ε is the *strain of standard C_0 finite elements*, interpolated from the *nodal displacements* $\mathbf{u}$ by the *strain operator* $\mathbf{B}$, and that $\tilde{\varepsilon}$ is the *enhanced part of strain* which is a function of the crack opening α inside this element.

Based on Eqs. (1a) and (2), we can write down the governing equations of the one-dimensional crack-embedded element in Fig. 5 by carefully emulating the governing equations of one-dimensional theory of plasticity (Simo and Hughes 1998):

(i) Elastic Stress-Strain Relationship

$$\sigma = E\,(\varepsilon - \tilde{\varepsilon}). \qquad (3a)$$

(ii) Flow Rule and Softening Rule

$$\begin{aligned}\dot{\tilde{\varepsilon}} &= G\,\dot{\alpha} = G\gamma, \\ \dot{\alpha} &= \gamma.\end{aligned} \qquad (3b)$$

(iii) Yield Condition

$$f(\sigma,\alpha) \equiv \dot{\sigma} - [\,\sigma_Y + K(\alpha)\,] \le 0. \tag{3c}$$

(iv) Kuhn-Tucker Complementarity Conditions

$$\gamma \ge 0, \quad f(\sigma,\alpha) \le 0, \quad \gamma f(\sigma,\alpha) = 0. \tag{3d}$$

(v) Consistency Condition

$$\gamma \dot{f}(\sigma,\alpha) = 0 \quad (\text{ if } f(\sigma,\alpha) = 0\,). \tag{3e}$$

In this model defined by the above equations, the crack starts cracking as the tensile stress reaches σ_c; the function $K(\alpha)$ defines a general (nonlinear) softening behavior of cracks. We emphasize that in an easy and systematic way, the algorithm developed here can solve a broad range of softening rules normally used for concrete fracture, for example, Shah et al. (1995, p. 124).

Observing the above equations, we can easily see: (1) the correspondence between $\tilde{\varepsilon}$ in crack-embedded element and *plastic strain* ε^p in plasticity, and (2) the only difference in their formulations is the *geometric* factor $G\ (= 1/L)$ in crack-embedded element:

$$\dot{\varepsilon}^p = \gamma \quad \text{vs.} \quad \dot{\tilde{\varepsilon}} = G\gamma. \tag{4}$$

We can solve the above equations in the same way with solving the corresponding equations in plasticity (Simo and Hughes 1998); the resulted rate solution is

$$\begin{cases} \dot{\sigma} = E\,\dot{\varepsilon} & \text{as } \gamma = 0, \\ \dot{\sigma} = \frac{E\,K'(\alpha)}{EG+K'(\alpha)}\,\dot{\varepsilon} & \text{as } \gamma > 0. \end{cases} \tag{5}$$

where $\dot{\varepsilon} \equiv \mathbb{B}\dot{\mathbf{u}}$. From the solution, *the stress-strain response of this model is also controlled by its size through the geometric factor* $G\ (= 1/L)$; this is one characteristic feature of softening materials.

The governing equations (3) share the identical structure to one-dimensional plasticity, in the next subsection we *develop a return-mapping algorithm for the one-dimensional crack-embedded element by following the established algorithms in computational plasticity* (Simo and Hughes 1998).

3.2 *Return-Mapping Algorithm for the One-Dimensional Crack-Embedded Element*

Although the governing equations (3) of the one-dimensional crack-embedded element share the identical structure with those of one-dimensional plasticity, there are two characteristic features that differentiate cracking problems from the classical plasticity normally presented in textbooks: (i) $K(\alpha)$ is a *softening* function ($K'(\alpha) \le 0$), and (ii) the parameter α is not a *field* quantity (point-by-point), but an *element* parameter (element-by-element). When we follow the well-established algorithms in computational plasticity, it is necessary to check every arguments if they need modification due to the two characteristic features.

3.2.1 *Incremental governing equations by the backward-Euler scheme*

Applying the backward-Euler scheme ($\square_{n+1} = \square_n + \dot{\square}_{n+1}\Delta t$) to the governing equations (3), we obtain the incremental relations

(i) Elastic Stress-Strain Relationship

$$\begin{aligned} \sigma_{n+1} &= E\,(\varepsilon_{n+1} - \tilde{\varepsilon}_{n+1}), \\ \varepsilon_{n+1} &= \varepsilon_n + \Delta\varepsilon_n. \end{aligned} \tag{6a}$$

(ii) Incremental Flow Rule and Softening Rule

$$\begin{aligned} \tilde{\varepsilon}_{n+1} &= \tilde{\varepsilon}_n + G\Delta\gamma, \\ \alpha_{n+1} &= \alpha_n + \Delta\gamma, \end{aligned} \tag{6b}$$

where $\Delta\gamma \equiv \gamma_{n+1}\Delta t \ge 0$.

(iii) Discrete Kuhn-Tucker Conditions

$$\begin{aligned} & f_{n+1} = \sigma_{n+1} - [\,\sigma_c + K(\alpha_{n+1})\,] \le 0, \\ & \Delta\gamma \ge 0, \\ & \Delta\gamma\, f_{n+1} = 0, \end{aligned} \tag{6c}$$

where $f_{n+1} \equiv f(\sigma_{n+1}, \alpha_{n+1})$.

Note that return-mapping algorithm is a *strain-driven* algorithm: we are given the driving variable $\Delta\varepsilon_n\ (= \mathbb{B}\Delta\mathbf{u}_n)$ for each incremental step, the numerical problem is to update all variables in a manner consistent with the cracking model defined by Eqs. (6).

3.2.2 *The trial elastic state*

Then we consider an auxiliary state obtained by *freezing cracking*; in other words, first we consider a purely elastic (trial) step defined by the following formulas which are solely determined by the initial conditions $\{\varepsilon_n, \tilde{\varepsilon}_n, \alpha_n\}$ and the *given* strain increment $\Delta\varepsilon_n$ (Simo and Hughes 1998, p. 35)

$$\begin{aligned} \sigma^{\text{trial}}_{n+1} &\equiv E\,(\varepsilon_{n+1} - \tilde{\varepsilon}_n) = \sigma_n + E\Delta\varepsilon_n, \\ \tilde{\varepsilon}^{\text{trial}}_{n+1} &\equiv \tilde{\varepsilon}_n, \\ \alpha^{\text{trial}}_{n+1} &\equiv \alpha_n, \\ f^{\text{trial}}_{n+1} &= \sigma^{\text{trial}}_{n+1} - [\,\sigma_c + K(\alpha_n)\,], \end{aligned} \tag{7}$$

where $f^{\text{trial}}_{n+1} \equiv f(\sigma^{\text{trial}}_{n+1}, \alpha^{\text{trial}}_{n+1})$.

3.2.3 *The algorithmic cracking/unloading condition*

The most crucial component in a return-mapping algorithm is an algorithmic cracking/unloading condition which is *solely defined by the trial elastic state.* It is here that the two features of cracking—its softening nature and the discreteness of α—play important roles.

Consider the function $K(\alpha)$ defining a softening curve, i.e., if $\alpha_2 > \alpha_1$, there is $K(\alpha_2) \leq K(\alpha_1)$, we shall need the allowable set of $K(\alpha)$ to be restricted by the assumption:

Assumption *The softening curve $K(\alpha)$ holds the following properties*

$$K(\alpha) \text{ is a } \textit{convex} \text{ function}, \tag{8a}$$

$$EG + K'(\alpha) > 0. \tag{8b}$$

Though not the most general assumption, convexity is a convenient condition which can be easily identified. Moreover, most of the softening curves used for concrete cracking belong to convex functions (Shah, Swartz, and Ouyang 1995, p. 124), convexity covers a broad range of softening curves.

Eq. (8b) can be explicitly written as

$$E/L + K'(\alpha) > 0 \tag{9}$$

for $G = 1/L$. This indicates that the *size* of element affects the validity of algorithm; for a given elastic modulus E and softening curve $K(\alpha)$, the size L has an upper bound $\min |E/K'(\alpha)|$. This condition coincides with that of *snap-back instability*.

Lemma *By virtue of the Assumption* (8)*, we have*

$$f_{n+1}^{\text{trial}} \geq f_{n+1}. \tag{10}$$

Then the discrete Kuhn-Tucker conditions (6c) and the preceding Lemma imply the following algorithmic equivalent of the cracking/unloading conditions.

Proposition *Cracking/unloading is solely decided from f_{n+1}^{trial} according to the conditions*

$$\begin{aligned} &f_{n+1}^{\text{trial}} \leq 0 \Rightarrow \text{elastic step} \Leftrightarrow \Delta\gamma = 0, \\ &f_{n+1}^{\text{trial}} > 0 \Rightarrow \text{cracking step} \Leftrightarrow \Delta\gamma > 0. \end{aligned} \tag{11}$$

The algorithmic cracking/unloading condition has been established.

3.2.4 *The return-mapping algorithm*

The algorithm is summarized as follows,

1. Database for this element $\{\alpha_n\}$ and for the (single) quadrature point $\{\varepsilon_n\}$.

2. Given the updated strain at the (single) quadrature point
$$\varepsilon_{n+1} = \varepsilon_n + \Delta\varepsilon_n. \tag{12}$$

3. Compute the trial elastic state
$$\sigma_{n+1}^{\text{trial}} \equiv E\,(\varepsilon_{n+1} - \bar{\varepsilon}_n), \tag{13a}$$
$$f_{n+1}^{\text{trial}} \equiv \sigma_{n+1}^{\text{trial}} - [\,\sigma_c + K(\alpha_n)\,]. \tag{13b}$$

4. Test for cracking/unloading

   IF $f_{n+1}^{\text{trial}} \leq 0$ THEN

   Elastic Step: set $\square_{n+1} = \square_{n+1}^{\text{trial}}$ & EXIT

   ELSE

   Cracking Step: proceed to step 5

   ENDIF

5. Solve $\Delta\gamma$ by
$$\begin{aligned} g(\Delta\gamma) \equiv \sigma_{n+1}^{\text{trial}} - E\Delta\gamma \\ -[\,\sigma_c + K(\alpha_n + \Delta\gamma)\,] = 0 \end{aligned} \tag{14}$$
   and update database
$$\alpha_{n+1} = \alpha_n + \Delta\gamma, \tag{15a}$$
$$\sigma_{n+1} = E(\varepsilon_{n+1} - G\alpha_{n+1}). \tag{15b}$$

3.2.5 *Algorithmic tangent stiffness matrix*

If the full Newton-Raphson method is used for solving the equilibrium equations of global system, algorithmic tangent stiffness matrix will be necessary to reach quadratic convergence. It can be systematically derived from the formulation developed in previous subsections. We present the results here without derivation:

$$\mathbf{k}_T{}_n^{(k)} = \mathbb{B}^{\mathrm{T}} \left(\left. \frac{d\Delta\sigma_n^{(k)}}{d\Delta\varepsilon_n^{(k)}} \right|_0 \right) \mathbb{B}L, \tag{16}$$

in which $\square_n^{(k)}$ represents the variable $\square$ at the iteration step k in the time step n, and

$$\left. \frac{d\Delta\sigma_n^{(k)}}{d\Delta\varepsilon_n^{(k)}} \right|_0 = \begin{cases} E & \text{elastic step}, \\ \frac{EK'(\alpha_n^{(k)})}{EG+K'(\alpha_n^{(k)})} & \text{cracking step}. \end{cases} \tag{17}$$

3.3 *Implementation of Damping*

Now let us consider the implementation of *stiffness-proportional damping* for the one-dimensional crack-embedded element (with unit area) shown in Fig. 6. A viscous dashpot is arranged in a parallel combination with the crack-embedded element such that the total stress σ_{tot} transmitted by the combined unit is equal to the summation of the elastic stress (force) σ and damping stress (force) σ_{vis}

$$\sigma_{\text{tot}} = \sigma + \sigma_{\text{vis}}. \tag{18}$$

We also specify that $\mathbf{F}^{\text{vis}} = \langle \sigma_{\text{tot}} \quad -\sigma_{\text{tot}} \rangle$ is the damping force vector of this element, $\dot{\mathbf{u}} = \langle \dot{u}_1 \; \dot{u}_2 \rangle$ is the nodal velocity vector, $\mathbf{k}_E$ is the elastic stiffness matrix which is a constant, and $\mathbf{k}_T$ is the tangent stiffness matrix which is a function of time.

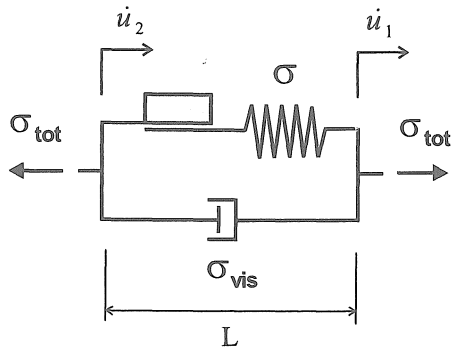

Figure 6: Damping Model

3.3.1 *Conventional implementation*

The conventional definition of stiffness-proportional damping can be expressed as

$$\sigma_{\text{vis}} = b_0 k(\dot{u}_1 - \dot{u}_2) \quad \text{or} \quad \mathbf{F}^{\text{vis}} = b_0 \mathbf{k}_E \dot{\mathbf{u}}. \tag{19}$$

When this element starts cracking, the deformation rate $\dot{u}_1 - \dot{u}_2$ can be accelerated without bound and the damping force significantly increases, by which the cracked element can transmit large tension by the mechanism of the damping force and trigger cracking of the neighboring elements. This implementation of damping causes unreal diffused cracks.

3.3.2 *Implementation by setting damping zero*

From the viewpoint of *implementing damping without altering the cracking behavior*, the best way could be to set the damping zero when the element starts cracking. Since the dashpot in Fig. 6 no longer exists, the crack-embedded element restores its original state in Fig. 5.

This approach may affect the stability of the numerical solution because damping forces change rapidly, and they can certainly reduce the convergence rate because the variation of damping is discontinuous that cannot be included in the algorithmic tangent stiffness matrix (Lee and Fenves 1998, p. 947).

3.3.3 *Implementation by tangent stiffness matrix*

Another way to implement damping for the crack-embedded element is to define the damping to be proportional to the *rate of elastic deformation*

$$\sigma_{\text{vis}} = b_0 k\,[\,\dot{u}_1 - \dot{u}_2 - \dot{\alpha}\,], \tag{20a}$$

$$= b_0 E\,[\,\mathbf{B}\dot{\mathbf{u}} - G\dot{\alpha}\,], \tag{20b}$$

where $\dot{\alpha}$ is the rate of crack opening. This approach is equivalent to define the damping force to be proportional to the tangent stiffness matrix

$$\mathbf{F}^{\text{vis}} = b_0 \mathbf{k}_T \dot{\mathbf{u}}. \tag{21}$$

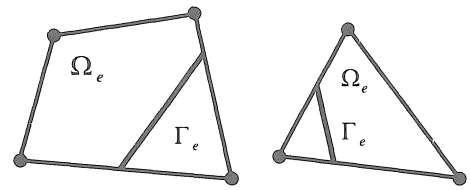

Figure 7: Two-Dimensional Crack-Embedded Elements

From the viewpoint of computation, this definition of damping is a continuous function of time which can be included in the tangent stiffness matrix as

$$\mathbf{k}_T^{\text{Damping}} = \left(1 + \frac{b_0}{\Delta t}\right) \mathbf{k}_T \tag{22}$$

in the backward-Euler scheme. The quadratic convergence rate of the full Newton-Raphson method is preserved.

On the other hand, the tangent stiffness of the crack-embedded element becomes negative as it is cracking, this approach more or less *accelerates* cracking by the negative damping (so changes the cracking behavior).

Both of the implementations by setting damping zero and by tangent stiffness matrix solve the problem of diffused cracking; they can be used as the alternative ways of implementing damping for the crack-embedded element.

3.4 *Extension to Two-Dimensional Crack-Embedded Elements*

Consider the two-dimensional crack-embedded elements shown in Fig. 7, they are the T3 and Q4 elements with domain Ω_e embedded with one crack Γ_e, respectively. Note that the crack opening $\boldsymbol{\alpha}_e$ is assumed to be *constant* inside each element (Oliver 1996; Armero and Garikipati 1996).

The general formulation of crack-embedded elements is based on the enhanced-strain elements (Simo and Rifai 1990) in which stress is expressed as

$$\boldsymbol{\sigma} = \mathbf{C}_e\,[\,\boldsymbol{\varepsilon} - \tilde{\boldsymbol{\varepsilon}}\,], \tag{23a}$$

$$= \mathbf{C}_e\,[\,\mathbf{B}_e\mathbf{u}_e - \mathbf{G}_e\boldsymbol{\alpha}_e\,], \tag{23b}$$

corresponding to Eqs. (1) for one-dimensional crack-embedded element. Note that the original form of this equation is $\boldsymbol{\sigma} = \mathbf{C}_e\,[\,\boldsymbol{\varepsilon} + \tilde{\boldsymbol{\varepsilon}}\,]$, we have changed the plus sign to minus one for following the convention of plasticity theory.

In the first sight, it might not be straightforward to formulate the "yield function" for two-dimensional cracked-embedded elements, because the element stress is a field quantity (e.g., Q4). In addition to

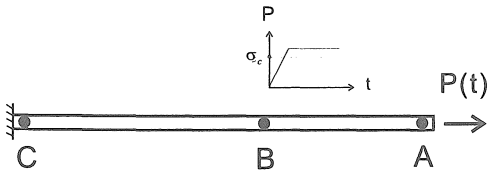

Figure 8: Rod Subject to Pure Tension

Eq. (23), the formulation of crack-embedded elements (Oliver 1996; Armero and Garikipati 1996) specifies a *weak condition of traction continuity* (in tensor notation)

$$\boldsymbol{\sigma}_{av} \cdot \mathbf{n} = \mathbf{T}_\Gamma(\alpha_e), \tag{24}$$

where $\mathbf{n}$ is the unit vector normal to the crack Γ_e, $\mathbf{T}_\Gamma$ is the cohesive stress inside the crack, and $\boldsymbol{\sigma}_{av}$ is the *average* stress tensor defined as

$$\boldsymbol{\sigma}_{av} \equiv \frac{1}{A_e} \int_{\Omega_e} \boldsymbol{\sigma}\, d\Omega, \tag{25}$$

where A_e is the area of the element.

We claim here without further presentation that by the specification of Eq. (24), we can formulate the corresponding "yield functions" corresponding to the opening mode (mode I) and sliding mode (mode II) of cracking and set up the complete governing equations with similar structure with Eqs. (3). Since the governing equations own a similar structure with those of one-dimensional plasticity (and the one-dimensional crack-embedded element), by emulating the well-established algorithms, we have proposed a *return-mapping algorithm for two-dimensional crack-embedded elements* in Chen and Horii (2001). The stiffness-proportional damping can be also implemented in the similar ways in Sec. 3.3.

3.5 *Examples*

In this section, two simple examples are presented for demonstrating the effects of damping implementation upon the computed results.

The first example is a one-dimensional rod (with unit area) which is subject to a pure tension force $P(t)$, shown in Fig. 8. The force initially increases linearly with time, then turns into constant when its magnitude slightly exceeds the tensile strength σ_c. For this problem, we can consider the following two stages. (1) Before the stress wave reaches the left end, all stress values generated by $P(t)$ are experienced earliest by the end A, therefore the end A is the first place to crack if $P(t)$ exceeds σ_c in this stage. Once the end A cracks, for the softening characteristic of cracking, it is no longer able to transmit stress higher than σ_c into the rod—no more cracks would occur after the end A does in this stage. (2) When the stress wave reaches the left end, the magnitude of the reflected wave is two times of that of the incident wave because of the rigid boundary. Hence if any pulse of $P(t)$ is higher than the half of σ_c, the end C cracks when this pulse reaches the left end. Same as the end A, once the end C cracks, it is no longer able to transmit stress higher than σ_c into the rod—no more cracks would occur by the reflected wave after the end C does. Consequently, we conclude that *only the end A and C is possible to crack in this problem.*

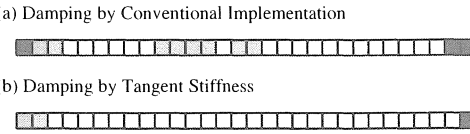

Figure 9: Results of the rod with different damping implementations: (a) cracked elements exist at the ends and inside, (b) cracked elements only exist at the ends

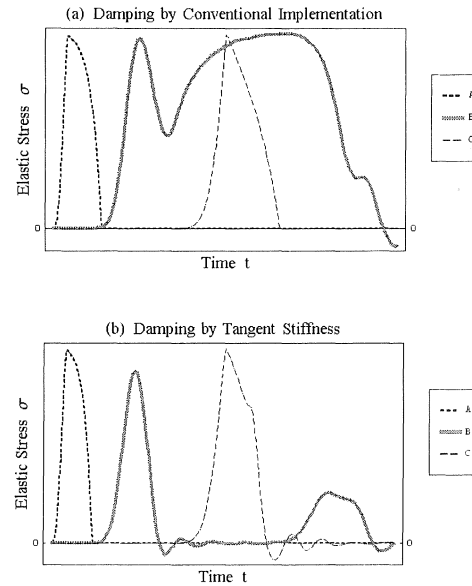

Figure 10: Stress Time-Variation of the Rod

The computed crack patterns are shown in Fig. 9 that the conventional implementation of damping not only generates cracks at the ends A and C but also generates a range of cracked elements inside the rod. We can see the reason by Fig. 10 where the time history curves of the stress at points A, B, and C are plotted; the point B is selected for it is an uncracked element. It is shown that the the point B can experience

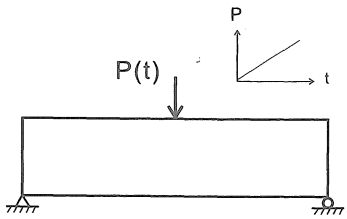

Figure 11: Three-Point Bending Test

high stress close to the tensile strength by the conventional implementation of damping. On the other hand, by implementing damping by tangent stiffness matrix the stress at the point B quickly damps out when both of the ends crack; only the ends A and C crack in this case.

The second example is a three-point bending test shown in Fig. 11, where a simply-supported beam is subject to a linearly increasing loading $P(t)$ at the center of its upper edge. The computed deformed shapes are shown in Fig. 12 that the conventional implementation of damping results in a zone of diffused cracks around the central bottom in which no obvious main crack is seen, whereas the damping implementation by tangent stiffness matrix obtains a more realistic localized main crack. The deflection of the former is less than that of the latter because the diffused cracking dissipates more energy during deflection—this implies a misleading stronger strength.

4 SUMMARY

When fracture mechanics of concrete is applied to the actual engineering problems, there would be requirements different from those for academic studies. In this paper, safety assessment of concrete dam against large earthquake is considered. The information provided by the dynamic analysis of crack growth in concrete for this purpose is the ligament ratio-earthquake intensity curve in Fig. 2. The reliability of this result is essential and its sensitivity to the crack modeling, input parameters, and so on must be carefully investigated. Issues discussed for the analysis of crack growth in concrete should be classified by the sensitivity to the result used in the solution of engineering problems.

In this paper, problems in crack modeling and damping implementation are reviewed because they strongly affect the ligament ratio-earthquake intensity curves. The simplicity of the discrete crack model could be more accessible for practicing engineers, for that the recently emerging crack-embedded elements are adopted. It is shown that the formulation of the crack-embedded element has an analogy with that of computational plasticity. This analogy enables us to utilize the return-mapping algorithm well established in computational plasticity for the dynamic analysis

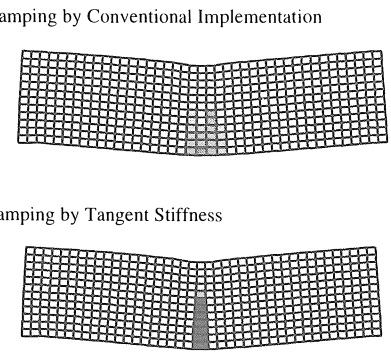

Figure 12: Result of the three-point bending test with different damping implementations: (a) diffused cracking, (b) localized cracking

of crack growth in concrete. The ways of implementing damping to avoid diffused cracking are presented and simple examples of numerical analysis are shown to demonstrate the effect of damping and the performance of appropriate damping implementation for cracked elements.

REFERENCES

Ariga, Y., S. Tsunoda, and H. Asaka (2000). Determination of dynamic properties of existing concrete gravity dam based on actual earthquake motions. 12WCEE, Paper No. 0334.

Armero, F. and K. Garikipati (1996). An analysis of strong discontinuities in multiplicative finite strain plasticity and their relation with the numerical simulation of strain localization in solids. *Int. J. Solids Structures 33*(20–22), 2863–2885. [Section 4].

Bhattacharjee, S. S. and P. Léger (1993). Seismic cracking and energy dissipation in concrete gravity dams. *Earthquake Engng. Struct. Dyn. 22*, 991–1007.

Cervera, M., J. Oliver, and R. Faria (1995). Seismic evaluation of concrete dams via continuum damage models. *Earthquake Engng. Struct. Dyn. 24*, 1225–1245.

Cervera, M., J. Oliver, and O. Manzoli (1996). A rate-dependent isotropic damage model for the seismic analysis of concrete dams. *Earthquake Engng. Struct. Dyn. 25*, 987–1010.

Chen, S.-C. and H. Horii (2001). A class of solution methods for crack-embedded elements by exploiting the return-mapping algorithm of computational plasticity. [in preparation].

Clough, R. W. and J. Penzien (1993). *Dynamics of Structures* (2nd ed.). McGraw-Hill, Inc.

El-Aidi, B. and J. F. Hall (1989). Non-linear earthquake response of concrete gravity dams, part 1: Modelling. *Earthquake Engng. Struct. Dyn. 18*, 837–851.

Faria, R., J. Oliver, and M. Cervera (1998). A strain-based plastic viscous-damage model for massive concrete structures. *Int. J. Solids Structures 35*(14), 1533–1558.

Ghaemian, M. and A. Ghobarah (1999). Nonlinear seismic response of concrete gravity dams with dam-reservoir interaction. *Engineering Structures 21*, 306–315.

Hillerborg, A., M. Modéer, and P. E. Petersson (1976). Analysis of crack formation and crack growth in concrete by means of fracture mechanics and finite elements. *Cement and Concrete Research 6*, 773–782.

Jirásek, M. (2000). Comparative study on finite elements with embedded discontinuities. *Comput. Methods in Appl. Mech. Engrg. 188*, 307–330.

Lee, J. and G. L. Fenves (1998). A plastic-damage concrete model for earthquake analysis of dams. *Earthquake Engng. Struct. Dyn. 27*, 937–956.

Léger, P. and M. Leclerc (1996). Evaluation of earthquake ground motions to predict cracking response of gravity dams. *Engineering Structures 18*(3), 227–239.

Oliver, J. (1996). Modelling strong discontinuities in solid mechanics via strain softening constitutive equations. part 2: Numerical simulation. *Int. J. Numer. Methods Eng. 39*, 3601–3623.

Shah, S. P., S. E. Swartz, and C. Ouyang (1995). *Fracture Mechanics of Concrete: Applications of Fracture Mechanics to Concrete, Rock, and Other Quasi-Brittle Materials*. John Wiley and Sons, Inc.

Simo, J. C. and T. J. R. Hughes (1998). *Computational Inelasticity*. Springer-Verlag New York, Inc. [Chapers 1–3].

Simo, J. C. and M. S. Rifai (1990). A class of mixed assumed strain methods and the method of incompatible modes. *Int. J. Numer. Methods Eng. 29*, 1595–1638.

Tinawi, R., P. Léger, M. Leclerc, and G. Cipolla (2000). Seismic safety of gravity dams: From shake table experiments to numerical analysis. *J. Struct. Engrg.*, ASCE *126*(4), 518–529.